RSC Advances

PAPER

View Article Online
View Journal | View Issue

Cite this: *RSC Adv.*, 2020, **10**, 12908

Insights into the promotion role of phosphorus doping on carbon as a metal-free catalyst for low-temperature selective catalytic reduction of NO with NH_3†

Weifeng Li,[a] Shuangling Jin,*[a] Rui Zhang,*[a] Yabin Wei,[a] Jiangcan Wang,[a] Shuo Yang,[a] He Wang,[a] Minghe Yang,[a] Yan Liu,[a] Wenming Qiao,[b] Licheng Ling[b] and Minglin Jin[a]

The catalytic reduction of NO with NH_3 (NH_3-SCR) on phosphorus-doped carbon aerogels (P-CAs) was studied in the temperature range of 100–200 °C. The P-CAs were prepared by a one-pot sol–gel method by using phosphoric acid as a phosphorus source followed by carbonization at 600–900 °C. A correlation between catalytic activity and surface P content is observed. The P-CA-800_{vac} sample obtained *via* carbonization at 800 °C and vacuum treatment at 380 °C shows the highest NO conversion of 45.6–76.8% at 100–200 °C under a gas hourly space velocity of 500 h^{-1} for the inlet gas mixture of 500 ppm NO, 500 ppm NH_3 and 5.0 vol% O_2. The coexistence of NH_3 and O_2 is essential for the high conversion of NO on the P-CA carbon catalysts, which can decrease the spillover of NO_2 and N_2O. The main Brønsted acid sites derived from P-doping and contributed by the C–OH group at edges of carbon sheets are beneficial for NH_3 adsorption. In addition, the C_3–P=O configuration seems to have the most active sites for favorable adsorption and dissociation of O_2 and facilitates the formation of NO_2. Therefore, the simultaneous presence of acidic groups for NH_3 adsorption and the C_3–P=O active sites for NO_2 generation due to the activation of O_2 molecules is likely responsible for the significant increase in the NH_3-SCR activity over the P–CAs. The transformation of C_3–P=O to C–O–P functional groups after the reaction is found, which could be assigned to the oxidation of C_3–P=O by the dissociated O*, resulting in an apparent decrease of catalytic activity for P-CAs. The C–O–P based functional groups are also active in the NH_3-SCR reaction.

Received 21st February 2020
Accepted 25th March 2020

DOI: 10.1039/d0ra01654c

rsc.li/rsc-advances

1. Introduction

In recent years, the widespread use of fossil fuels has produced nitrogen oxides (NO_x, mainly NO and NO_2) that cause serious environmental problems, such as acid rain, photochemical smog, and particulate matter formation.[1,2] Selective catalytic reduction of NO with NH_3 (NH_3-SCR) is a widely used technique for NO emission control during industrial production, with which an expensive and toxic V_2O_5–WO_3/TiO_2 catalyst is usually used. However, the optimum operating temperature of the V_2O_5–WO_3/TiO_2 catalyst is high (300–400 °C), so the SCR device must be installed upstream of the desulfurizer and dust collector to avoid reheating the flue gas, which shortened service life of the catalyst by the deactivation from the poisoners of high-concentration SO_2 and dust.[3–5] The difficulty in recovery of toxic vanadium species from the TiO_2 support is another problem for this catalyst system. Therefore, the development of environment-friendly catalysts with high catalytic activity at relatively low temperature (100–200 °C) has become a research hotpot.

Carbon materials have been attracted great attention owning to their adjustable physical characteristics and surface chemistry properties. Except being used as the supports for the metal-based catalysts, carbon materials can also act as the metal-free catalysts by doping heteroatoms such as oxygen (O), nitrogen (N), boron (B), sulfur (S), and phosphorus (P), to tailor the electron donor–acceptor properties of carbon matrix. Oxygen, is the most common heteroatom on edges of carbon sheets, whose effects on the catalytic activity of carbon-based catalysts for NO reduction have been extensively studied. Many researchers have shown that the catalytic activity of carbon materials for NO conversion increases with the numbers and kinds of surface oxygen groups, as the adsorption sites for NO and NH_3 molecules.[6–9] Recently, Zhang *et al.* proposed that the

[a]*School of Materials Science and Engineering, Shanghai Institute of Technology, Shanghai, 201418, PR China. E-mail: jinshuangling@sit.edu.cn; zhangrui@sit.edu.cn*
[b]*State Key Laboratory of Chemical Engineering, East China University of Science and Technology, Shanghai, 200237, China*

† Electronic supplementary information (ESI) available. See DOI: 10.1039/d0ra01654c

carboxylic acid groups can directly participate in NO reduction.[10] In addition, some studies have indicated that the incorporation of N into the carbon sheets can enhance the NH_3-SCR activity.[11–14] It is speculated that the nitrogen species can increase the carbon basicity and create the extra delocalized electrons for easy chemisorption of weakly acidic NO and O_2 to facilitate NO_2 formation.[11,12] The NO conversion can be increased effectively by nitrogen-doping for the pre-oxidized carbon samples, suggesting the presence of acidic surface groups and N-containing functional groups is important for the activity and the selectivity of N_2.[11,12] Moreover, experimental and theoretical studies have revealed that N or S-doped graphene can be applied for direct catalytic decomposition of NO, the surface functional groups play a key role. The unique functional groups (pyridinic N and thiophene S) can transfer extra electrons to the π-antibond orbital of NO, which leads to lengthening the length of N-O bonds and reducing the order of N–O bonds, thereby weakening the NO stability. Eventually, the formation of N_{ads} and O_{ads} would further form N_2 and O_2. But the reaction temperature is pretty high (600–850 °C), which resulted in graphene oxidation that limit its long-term stability.[15–18] Ji *et al.* systematically explored the possibility of boron-doped graphene (BG) for the NO electrochemical reduction (NOER) reaction through density functional theory (DFT). The results showed the introduction of B atom enhances the interaction of graphene with the HNO* intermediate, in which the preferable NO → HNO* → NH_2O* → NH_2OH* → NH_2* → NH_3 with a limiting potential of −0.35 V.[19]

P, situated in the same main group as N, possesses the same number of valence electrons as nitrogen. But it has a larger atomic radius and higher electron-donating ability than nitrogen, which make it an interesting dopant to alter the surface chemical properties of carbon sheets in specific applications.[20–23] P modification can increase the specific capacitance of carbon electrode materials by the additional faradaic redox reactions, improve the cycle stability and widen the potential window as an oxidation protector in supercapacitors.[23,24] The P-doped carbon materials as metal-free electrodes have exhibited higher electrocatalytic activity, lower resistance and much higher stability than commercial Pt/C catalysts for oxygen reduction reactions (ORR) in methanol oxidation.[20,21,25–29] The P-doped carbon can be used as a metal-free catalyst to efficiently catalyze aerobic oxidation of benzyl alcohols to aldehydes or ketones.[21] In addition, similar to nitrogen doping, the P-doping of carbon can increase the catalytic selectivity to alkene and decrease the consumption of hydrocarbons as a metal-free catalyst for selective hydrogenation of hydrocarbons.[30,31] Furthermore, the catalytic role of phosphorus oxide clusters on carbon surface for alkane oxidative dehydrogenation was reported recently by Huang *et al.*[32] They found that the P═O configurations, exhibiting the structure and reactivity features similar to those of the traditional active metal oxide clusters, tended to abstract hydrogen atoms and favored the alkene selectivity. Despite multiple advantages of P-doping shown in above application fields, to the best of our knowledge, the effects of P-doping on the NH_3-SCR performance of carbon-based catalysts is seldom concerned and the underlying principles remain unknown.

In the present work, P-doped carbon aerogels (P-CAs) were prepared by a one-pot sol–gel method using phosphoric acid as the phosphorus source, followed by carbonization at 600–900 °C. The contributions of P-containing functional groups to the NH_3-SCR performance of the P-CAs at low temperatures (120–200 °C) were systematically investigated and discussed. We expect that these findings can broaden the insights into contributions of heteroatom-doping in carbon for NO reduction.

2. Experimental section

2.1 Catalyst preparation

In a typical synthesis, 8.15 g of phenol and 1.87 g of *m*-cresol were dissolved in 100 mL of 1-propanol to form a solution, then 2.98 g of phosphoric acid (85 wt%) was added to the solution under stirring and heated at 70 °C for 1 h. After the above solution was cooled to room temperature, 19.97 g of furfural was added to the solution under agitating for 15 min. The obtained mixed solution was poured into several ampules (30 mL), sealed, placed in a water bath at 80 °C for 5 days, and then at room temperature for 1 day, finally dried at 60 °C to obtain cylindrical organic xerogels. At last, the organic xerogels were carbonized in a vertical tube furnace at 600 °C, 700 °C, 800 °C and 900 °C for 3 h with a heating rate of 5 °C min^{-1} in nitrogen atmosphere, to obtain the P-CAs, which were denoted as P-CA-*x*, where *x* represents the carbonization temperature. Meanwhile, the P-CA-800 sample was subjected to heat treatment at 380 °C for 8 h in vacuum to obtain sample P-CA-800_{vac}. For comparison, the P-free carbon aerogel was prepared following the same procedures and formulation without adding phosphoric acid under a carbonization temperature of 800 °C, which was denoted as CA-800.

2.2 Characterization of catalysts

The pore texture of the P-CAs and CA-800 was characterized by N_2 adsorption at 77 K (Micromeritics, ASAP-2020). Samples were out-gassed at 150 °C for 12 h in vacuum prior to the measurements. The surface areas (S_{BET}) was determined by the Brunauer–Emmett–Teller (BET) method using the N_2 adsorption data. The mesopore volumes (V_{mes}) and micropore volumes (V_{mic}) were evaluated by the density functional theory (DFT) model. Surface compositions of samples were analyzed by X-ray photoelectron spectroscopy on a Thermo Scientific Escalab 250Xi system. The corresponding binding energies were calibrated by using C1s of 284.8 eV as a standard. The P content on the surface of samples was also examined by inductively coupled plasma atomic emission spectrometry (ICP-AES) on an Agilent 720 apparatus, in which the samples were digested by a microwave assisted pre-treatment. Fourier transform infrared (FTIR) spectra were recorded on a Nicolet Nexus 410 spectrometer at the range of 4000–400 cm^{-1} with a resolution of 4 cm^{-1} by collecting 256 scans. NH_3-temperature programmed desorption (NH_3-TPD) experiments were performed on

a Micrometrics AutoChem II 2920 instrument. 100 mg of sample was pre-treated at 300 °C for 1 h in N_2 and cooled to 50 °C, then was saturated with a 10 vol% NH_3/Ar gas mixture at a flow rate of 30 mL min^{-1} for 1 h, followed by N_2 purge for another 0.5 h, finally raised to 500 °C at a heating rate of 10 °C min^{-1} to obtain the NH_3-TPD curves.

2.3 Catalytic activity measurement

The NH_3-SCR activities were measured in a fixed-bed glass reactor with an internal diameter of 15 mm. The mass of the catalyst in the fixed-bed was 3.61 g. The simulated flue gas was composed of 500 ppm NO, 500 ppm NH_3, 5.0 vol% O_2, and N_2 as the balance gas at a total flow rate of 88 mL min^{-1}, corresponding to the gas hourly space velocity (GHSV) of 500 h^{-1}. The catalytic reaction was tested from 100 to 200 °C. The outlet concentration of NO and NO_2 were measured by a chemiluminescence method with an ECO PHYSICS nCLD62s NO/NO_x analyzer and the concentration of N_2O was detected by gas chromatography with a Techcomp GC 7900 equipment. The concentration of NH_3 was measured by a laser method on a Mic-500S–NH_3-Tdlas NH_3 analyzer. The NO conversion was calculated using the following eqn (1),

$$x = \frac{C(NO_x)_{in} - C(NO_x)_{out}}{C(NO_x)_{in}} \quad (1)$$

where the concentrations of NO_x in the inlet and outlet are represented by $C(NO_x)_{in}$ and $C(NO_x)_{out}$, respectively.

In this work, to better evaluate the catalytic activity of the P-CAs and CA-800, a steady state kinetics investigation of the catalysts was conducted. The calculation of the reaction rate constant k in the kinetics equation was based on the assumptions that the reaction is first order dependence of NO and zero order dependence of NH_3.[33,34] The calculation formula shown in the eqn (2):

$$k = \frac{-Q\ln(1-x)}{W} \quad (2)$$

where k is the reaction rate constant ($cm^3\ g^{-1}\ s^{-1}$), Q means the total gas flow (mL min^{-1}), W is the mass of the catalyst in the fixed reaction bed (g) and x is the NO conversion. The apparent activation energy of the reaction is calculated according to the Arrhenius eqn (3):

$$k = Ae^{\frac{-E_a}{RT}} \quad (3)$$

where E_a (kJ mol^{-1}) represents the apparent activation energy of catalyst, which could be calculated from the slope of the curve $\ln(k)$ *versus* $1/T$.

3. Results and discussion

XPS measurements were used to characterize the types and contents of P-containing groups on the surface of as-obtained P-CAs. As shown in Fig. S1,† the peaks at 132.9 eV, 284.8 eV and 532.6 eV on the XPS full spectra of the P-CAs are assigned to P2p, C1s and O1s, respectively. The corresponding atomic contents of P, C and O are calculated and listed in Table 1. With increasing the carbonization temperature, the P content on the surface of carbon aerogels increases, reaching the highest value of 2.50% for the P-CA-800 sample, and then decreases to 1.37% for the sample P-CA-900. Meanwhile, the P content of the samples is also examined by ICP-AES and listed in Table 1. It is shown that the changing trend of the ICP results with the carbonization temperature is consistent with that of the XPS measurements. The ICP results represent the global atomic contents while the XPS measurements the surface atomic contents that depend on the penetration depth of XPS.

Table 1 Atomic compositions of the P-CAs

	XPS analysis			ICP analysis
Sample	C (%)	P_{XPS} (%)	O (%)	P_{ICP} (%)
P-CA-600	87.87	2.21	9.92	2.30
P-CA-700	91.74	2.31	5.95	3.01
P-CA-800	90.83	2.50	6.67	3.28
P-CA-800$_{vac}$	90.38	2.22	7.40	2.34
P-CA-900	90.94	1.37	7.69	1.64

The high-resolution P2p spectra can be fitted to four peaks at 130.2 eV, 132.2 ± 0.4 eV, 134.0 ± 0.2 eV and 136 ± 0.5 eV, which corresponds to C_3–P, C_3–P=O, C–O–P, and phosphorus pentoxide (P_2O_5),[35–38] respectively, as shown in Fig. 1. It can be seen that the contents of C_3–P, C_3–P=O and P_2O_5 increase, whereas that of C–O–P decrease with increasing the carbonization temperature before 800 °C. The formation of more C_3–P and C_3–P=O (sum of the two) configurations at a higher carbonization temperature indicates that more P atoms are doped into the C–C lattice at a higher carbonization temperature.[39] But thermal decomposition of the C_3–P=O group is found beyond 800 °C (the sample P-CA-900). It is reported that the presence of P_2O_5 may result in the pore blocking that affects the surface activity of carbon.[40] Therefore, the P-CA-800 sample was subjected to heat treatment at 380 °C for 8 h under vacuum to obtain sample P-CA-800$_{vac}$. It is shown that P_2O_5 can be successfully sublimed during the vacuum treatment. Meanwhile, the C_3–P configuration also vanishes, which may be attributed to the fact that the transformation of C_3–P into C_3–P=O during the vacuum treatment *via* interaction with a trace amount of oxygen because of the lower formation energy of C_3–P=O and its highly stable structure.[24] The O1s spectra can be deconvoluted into four peaks located at 531.2 ± 0.2 eV, 532.5 ± 0.3 eV, 533.5 ± 0.2 eV and 534.9 ± 0.2 eV, which are assigned to C=O and P=O, C–O–C and C–O–P, C–OH and P–OH, and carboxylic groups COOH and/or H_2O, respectively.[22,23,35,40] The P–OH groups may be mainly linked on the C–O–P structure as the forms of CO–$P(O)(OH)_2$ and $(CO)_2$–P(O)(OH) groups located at the edge of graphene layer.[41] It is shown that the relative proportion of O_1 increases firstly and then decreases with increasing the carbonization temperature, in consistence with the evolution of C_3–P=O. The concentrations of O_3 and O_4 decrease gradually with the rise of the carbonization temperature due to their instability at high temperatures.

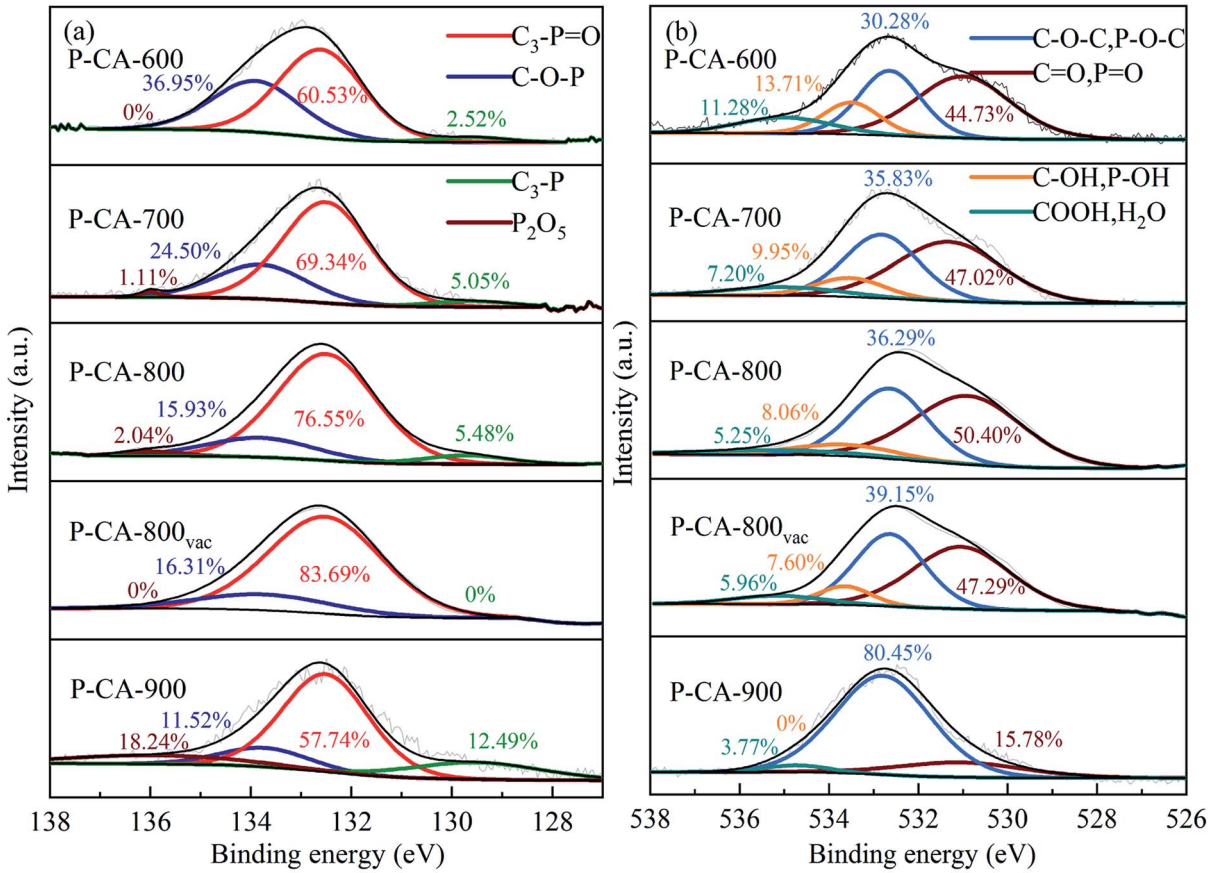

Fig. 1 The deconvoluted and the fitted results of (a) P2p and (b) O1s spectra of the P-CAs.

The pore textures of the CA-800 and P-CAs were analyzed by N_2 adsorption, as shown in Fig. S2a,† the adsorption isotherms of all samples exhibit a typical type II isotherm curve with a H_3 hysteresis loop, indicating the existence of mesopores in the texture. Meanwhile, the high nitrogen uptakes at a low relative pressure and a high relative pressure above 0.95 can be observed due to the coexistence of micropores and macropores, in consistence with the corresponding pore size distributions displayed in Fig. S2b.† As displayed in Table 2, the BET surface area and total pore volume of the P-CAs decrease gradually with increasing the carbonization temperature from 600 to 900 °C, which are lower than that of the CA-800. It is worth noting that the specific surface area of the P-CA-800$_{vac}$ is significantly higher than that of the P-CA-800 due to the removal of P_2O_5 that is mainly filled in the micropores, resulting in the distinct increase of micropore volume.

NH_3-TPD tests were used to explore the number and intensity of acid sites on the obtained samples. As shown in Fig. 2, a distinct NH_3 desorption peak at 100–250 °C is observed from the TPD profiles of the P-CA-800 and P-CA-800$_{vac}$ samples, whereas no obvious peak is detected for the CA-800 sample. The NH_3 adsorption amounts for the P-CA-800 and P-CA-800$_{vac}$ are higher than that of the CA-800. It is generally believed that the peaks below 400 °C on the NH_3-TPD profiles is attributed to NH_4^+ ions coordinated on the Brønsted acid sites and the NH_3 molecule is coordinated to the Lewis acid sites above 400 °C.[42–44] The Brønsted acidity may be originated mainly from the surface C–OH (CA-800, P-CA-800 and P-CA-800$_{vac}$) and P–OH (P-CA-800 and P-CA-800$_{vac}$) groups revealed by above XPS analysis, which

Table 2 Textual parameters of the CA-800 and P-CAs

Samples	S_{BET} ($m^2\ g^{-1}$)	V_{total} ($m^3\ g^{-1}$)	V_{mes} ($m^3\ g^{-1}$)	V_{mic} ($m^3\ g^{-1}$)
P-CA-600	367	0.763	0.244	0.097
P-CA-700	323	0.695	0.234	0.077
P-CA-800	217	0.625	0.217	0.055
P-CA-800$_{vac}$	315	0.673	0.221	0.080
P-CA-900	202	0.597	0.222	0.059
CA-800	447	0.768	0.597	0.118

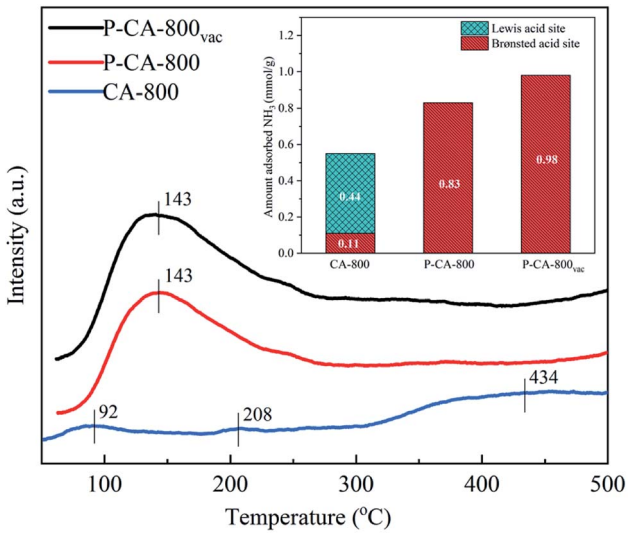

Fig. 2 NH_3-TPD profiles and the corresponding amounts of adsorbed NH_3 over the CA-800, P-CA-800 and P-CA-800_{vac}.

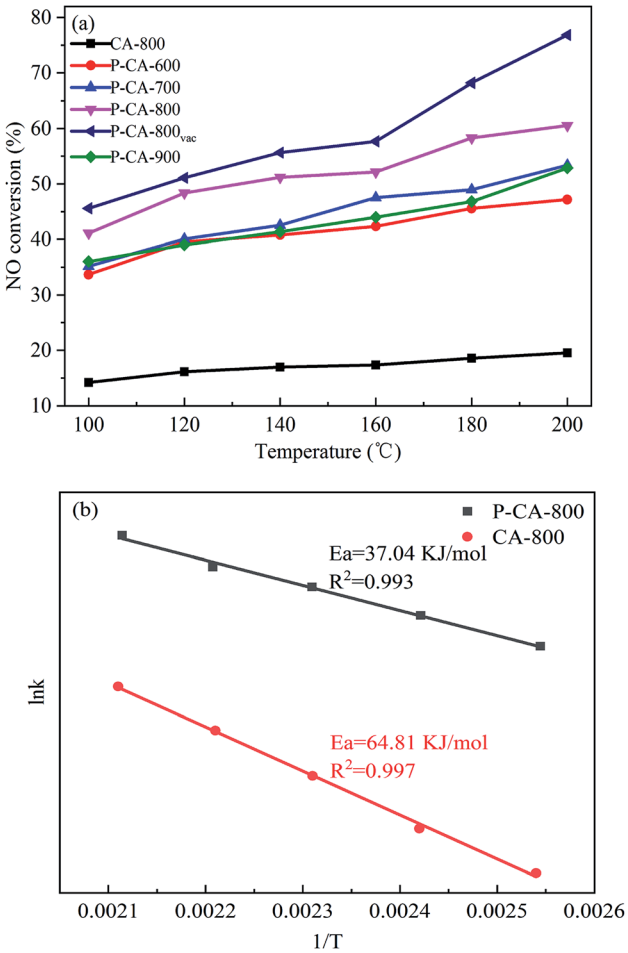

Fig. 3 (a) NO conversions over the CA-800 and P-CAs (reaction conditions: [NO] = 500 ppm, $[NH_3]$ = 500 ppm, $[O_2]$ = 5%, N_2 balance, GHSV = 500 h^{-1}) and (b) Arrhenius plots of the P-CA-800 and CA-800 samples.

are favorable for coordination with NH_3 to form NH_4^+ and facilitate the NH_3-SCR reaction.[9,45–49] It is worth noting that the Lewis acid sites of P-CA-800 and P-CA-800_{vac} samples disappeared and the number of Brønsted acid sites increased significantly. This is because phosphoric acid can inhibit the generation of strong acid sites and generate weak acid sites.[50] The COOH group is unstable at a high temperature, therefore the contribution of COOH group to the Brønsted acid sites is less obvious than that of C–OH and P–OH groups. After the vacuum treatment at 380 °C for 8 h, more Brønsted acid sites are exposed as a result of removal of P_2O_5 by sublimation as shown in Fig. 2. So the amount of adsorbed NH_3 follows the order, CA-800 < P-CA-800 < P-CA-800_{vac}.

The NH_3-SCR performance of the P-CAs were examined and shown in Fig. 3a. It is interesting to note that all the P-CAs exhibit higher catalytic activity for NO reduction compared with that of the CA-800. It is noted that the catalytic activity of the P-CAs is related to their surface P contents. The NO conversion over the P-CA-800 sample is 41.1–60.6% in the temperature range of 100–200 °C, whereas it is only 14.2–19.5% for the CA-800. To further compare the catalytic performance of the CA-800 and P-CA-800, their Arrhenius plots are tested and the corresponding apparent activation energies (E_a) are calculated from kinetics study, as displayed in Fig. 3b. The apparent activation energy of the P-CA-800 (37.04 kJ mol^{-1}) is significantly lower than that of CA-800 (64.81 kJ mol^{-1}), in accordance with their catalytic activity. In addition, it is shown that the catalytic activity of the P-CA-800_{vac} is improved significantly compared with that of the P-CA-800, which is 45.6–76.8% at 100–200 °C, suggesting more active sites are exposed after the vacuum treatment.

In order to explore the promotion effects of P-doping on the NH_3-SCR performance, the fresh P-CA-800_{vac} sample was subjected to NH_3-SCR reaction at 120, 140, 160, 180, 200 °C for 1 h to obtain P-CA-800_{vac}-120, P-CA-800_{vac}-140, P-CA-800_{vac}-160, P-CA-800_{vac}-180, P-CA-800_{vac}-200, respectively. The XPS analysis results of above used samples are shown in Fig. S3† and Table 3. It can be clearly seen that the content of C decreases, the content of O increases, whereas the content of P is almost unchanged for the used samples compared with that of the fresh P-CA-800_{vac} sample, indicating that the increase of oxygen can be regarded as the adsorption of NO on the catalyst surface during the NH_3-SCR reaction. It is worth noting that oxygen

Table 3 Atomic compositions of the P-CA-800_{vac} after the NH_3-SCR reaction for 1 h at different temperatures as examined by XPS

	XPS analysis		
Sample	C	O	P
P-CA-800_{vac}-120	81.23	16.59	2.18
P-CA-800_{vac}-140	77.26	20.55	2.19
P-CA-800_{vac}-160	75.42	22.43	2.15
P-CA-800_{vac}-180	70.14	27.68	2.18
P-CA-800_{vac}-200	65.77	32.06	2.17

content in XPS results have a linear relationship with the removal efficiency of NO.

The P2p and O1s spectra and the corresponding deconvoluted results are shown in Fig. S4† and 4. It can be observed from the P2p spectra that the content of C_3–P=O decreases rapidly, while the content of C–O–P gradually increases with increasing the reaction temperature. The O1s spectra indicate that the –OH and COOH groups all disappear after reaction, which may be due to the oxidation of –OH to ketones and the consumption of COOH during reaction.[10] It should be mentioned that the contribution of carboxylic acid groups to NO reduction is minor due to their low concentration, although the carboxylic acid groups can directly react with NO.[10] The decrease in the contents of C=O and P=O, and the increase in the contents of C–O–C and P–O–C groups can be observed from the O1s spectra, indicating the oxygen have entered the C–P bond and/or the C–C bond during reaction.

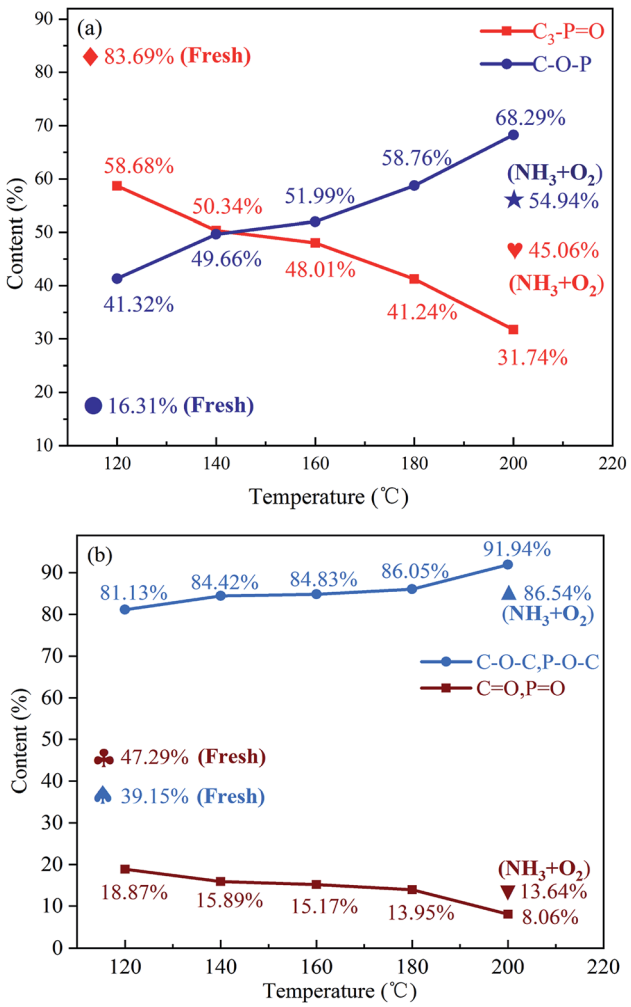

Fig. 4 Relative surface concentrations of phosphorous species for the P-CA-800_{vac} sample after the NH_3-SCR at different reaction temperatures obtained from (a) P2p XPS spectra and (b) O1s XPS spectra. Reaction conditions: [NO] = 500 ppm, [NH_3] = 500 ppm, [O_2] = 5%, N_2 balance, GHSV = 500 h^{-1}.

The P-CA-800_{vac} sample was also treated in a mixed gas of NH_3 and O_2 at 200 °C for 1 h and then subjected to XPS test. It is shown that a part of C_3–P=O can also be transferred into C–O–P functional group without NO atmosphere, although the conversion of C_3–P=O is less than that of the used P-CA-800_{vac} sample after reaction in NO + NH_3 + O_2 atmosphere, indicating that the presence of NO accelerates the oxidation of the C_3–P=O group.

FTIR spectra were also used to detect the change of surface composition for the P-CA-800_{vac} samples before and after the NH_3-SCR reaction at different temperatures, as shown in Fig. 5. A strong broad absorption band at 3450 cm^{-1} (hydroxyl groups and/or the adsorbed water), a minor peak at 2960, 2920 and 2850 cm^{-1} (C–H stretching in CH_2), an absorption band at 1580 cm^{-1} (C=C stretching in aromatic ring), and an absorption band at 1480–1400 cm^{-1} (bending modes from CH_2, CH_3, and OH) are observed for all the samples.[51–53] In addition, a broad absorption band at 1300–900 cm^{-1} is observed, which should be attributed to the overlapping signals for vibration of oxygen and phosphorus functional groups. The peak at 1180 cm^{-1} is generally assigned to stretching vibration from P=O, C–O in C–O–P, and O=P–OH,[54] and the band at 1115 cm^{-1} to bending vibration of C–O–C group.[55] The absorption signals in this region become stronger after the NH_3-SCR reaction, indicating that more C–O–C and/or C–O–P functional groups are generated during reaction, which is consistent with above XPS analysis results.

The long-term stability of the P-CA-800_{vac} sample for the NH_3-SCR reaction was further evaluated, as shown in Fig. 6a. The NO conversion maintains at *ca.* 77% during the first 14 h, which then decreases sharply to *ca.* 40% for the rest of test time. The P2p and O1s XPS results of the used sample after stability test show that most of the C_3–P=O configurations on the catalyst surface have been converted into C–O–P groups (Fig. 6b and c), suggesting that the C_3–P=O groups may be the active sites for the high NH_3-SCR activity of the P–CAs. The sudden deactivation of the catalyst at the fourteenth hour may be due to the fact that the C_3–P=O groups gradually converted to C–O–P groups that are less active after NH_3-SCR reactions for 14 h. At the 14 h, the number of C_3–P=O groups as active sites became too small to maintain the high NH_3-SCR activity of the P-CA-800_{vac}, resulting in a partial deactivation of the catalyst. The C_3–P=O group decreases by 88% after reaction for 14 h while the NH_3-SCR activity decreases by 63% of the original level. The remaining activity may be due to the Brønsted acid sites contributed by the C–O–P groups ($(CO)P(O)(OH)_2$ and $(CO)_2$–P(O)(OH) groups) that are active in NH_3-SCR reaction.

The above results show that P-doping significantly enhances the NH_3-SCR activity of carbon aerogels as a metal-free catalyst, and the C_3–P=O structure seems to be the most active sites for the reaction. To explore the possible mechanism for NO reduction on P-CA surface, the NO conversions, NO_2 and N_2O concentrations in the outlet gas over the P-CA-800_{vac} sample under NO, NO + O_2 and NO + NH_3 + O_2 atmosphere at 100–200 °C were also tested, as shown in Fig. 7. It should be mentioned that NH_3 can not be detected in the tail gas under the atmosphere of NO + NH_3 + O_2, which may be due to the

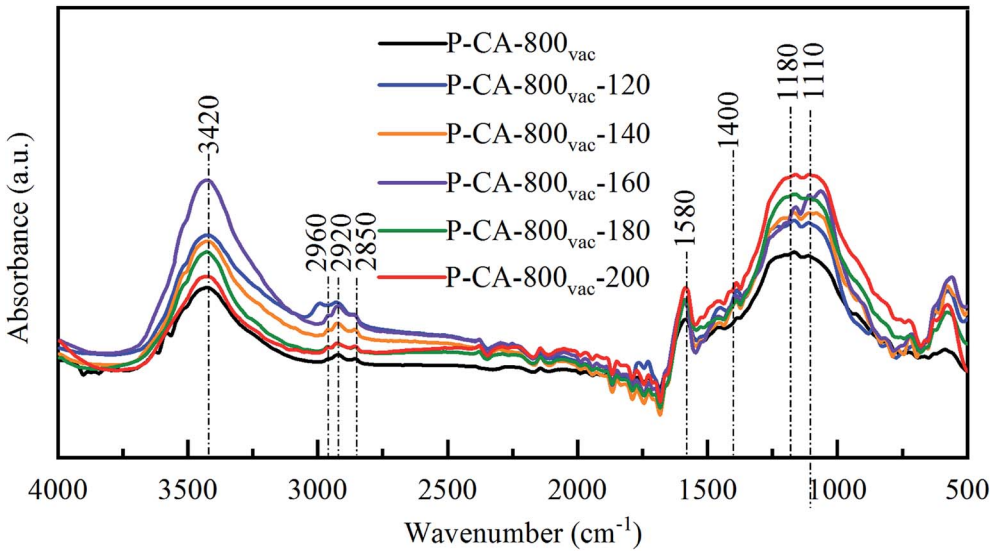

Fig. 5 FTIR spectra of the P-CA-800$_{vac}$ samples before and after the NH_3-SCR reaction for 1 h at different temperatures.

adsorption of NH_3 on the acid sites and the subsequent consumption *via* reaction. It is shown that the NO removal efficiency is in the order of NO + NH_3 + O_2 > NO + O_2 > NO, demonstrating that the coexistence of NH_3 and O_2 is essential for the high conversion of NO on the P-CAs.

Molecule NO contains an unpaired π-antibonding orbit and prefers to accept electron from substrates.[17] The density functional theory (DFT) calculations have shown that NO molecule can be adsorbed moderately on the P-doped carbon surface due to the electron-donating nature of P atom that can create localized electronic state into the carbon skeleton.[56] The electron transfer from P-doped carbon to NO molecule could elongate N–O bond length and decrease N–O bond order.[56] The mechanisms for the adsorption and decomposition of NO on the N-doped graphene (NG) have been studied by the DFT calculations.[15,16] It is reported that the dimer mechanism is more facile than the direct dissociation NO to N* and O*, which involves the adsorption of two NO molecules on the surface of NG, followed by the decomposition of $(NO)_2$ dimer into N_2O and adsorbed O*, then N_2O can dissociate to N_2 and adsorbed O* and NO can react with adsorbed O* to form NO_2, as depicted in the eqn (4)–(7). The catalytic reduction of NO on the P-CAs is proposed to follow the above dimer mechanism, because NO_2 and N_2O are detected in the outlet gas when the P-CA-800$_{vac}$ is exposed to only NO diluted in N_2, as shown in Fig. 7a.

The depletion efficiency of NO is enhanced when O_2 is introduced into the system compared with the situation when NO is solely present in the inlet gas, as shown in Fig. 7b. It is shown that the NO_2 concentration in the tail gas is also higher under the atmosphere of NO + O_2 than the NO atmosphere, indicating that the presence of O_2 may facilitate the oxidation of NO to NO_2. The catalytic oxidation mechanisms of NO ($2NO + O_2 \rightarrow 2NO_2$) over carbon have been studied extensively in the last decades,[57–59] namely, Eley–Rideal (E–R) and Langmuir–Hinshelwood (L–H) mechanisms are proposed. For the L–H mechanism, adsorbed NO reacts with dissociated O* activated by carbon, and for the E–R mechanism, gaseous NO and O_2 directly reacts in narrow micropores.[60–62] By comparing P-CA-800 and P-CA-800$_{vac}$ catalysts, we can find that there are more phosphorus-containing functional groups on the exposed surface of P-CA-800$_{vac}$ catalysts, and at the same time, partially blocked micropores by P_2O_5 are released, which may provide another routine for denitration by reactions of gaseous NO and O_2 in the micropores,[61] thereby improving the denitration efficiency of the catalyst. However, very few micropores are present in the P-CAs as demonstrated from the N_2 adsorption results, hence the existence of micropores can only promote the oxidation of NO and is not a key factor affecting the denitrification mechanism of catalyst. So, we considered that the enhanced NO oxidation activity should be attributed to the P-doping on carbon surface, which may facilitate the adsorption and dissociation of O_2 molecule that have been revealed in ORR process.[21,25–29] Due to the difference of electron negativity between heteroatoms and carbon, the incorporation of heteroatoms can cause charge redistribution of carbon skeletons to create charged sites favorable for O_2 adsorption. The catalytic active sites in the P-doped carbon are believed to be the positively charged P atoms because the electronegativity of P (2.19) is less than that of carbon (2.55) on the basis of three-coordinated P-doped graphene (PC3G) structure.[21,28] In present work, the dominant active sites should be C_3–P═O, in which the dangling-bond of P atom is saturated by O atom, making the adjacent C atoms become the sole active sites for O_2 adsorption.[25–27,29] The O atom with the highest electronegativity (3.44) will redistribute atomic charge of (PC3G) structure, namely, O and P atom can coordinate to adjust the electrons of C atom by using P atom as a connector. As a result, although the C atoms exhibit negative charge, they can also be the optimal active sites for favorable adsorption and dissociation of O_2 according to the DFT calculation results,[29] as described in the eqn (8). The presence of O_2 can promote the generation of NO_2 and reduce the spillover of N_2O, which is also consistent with

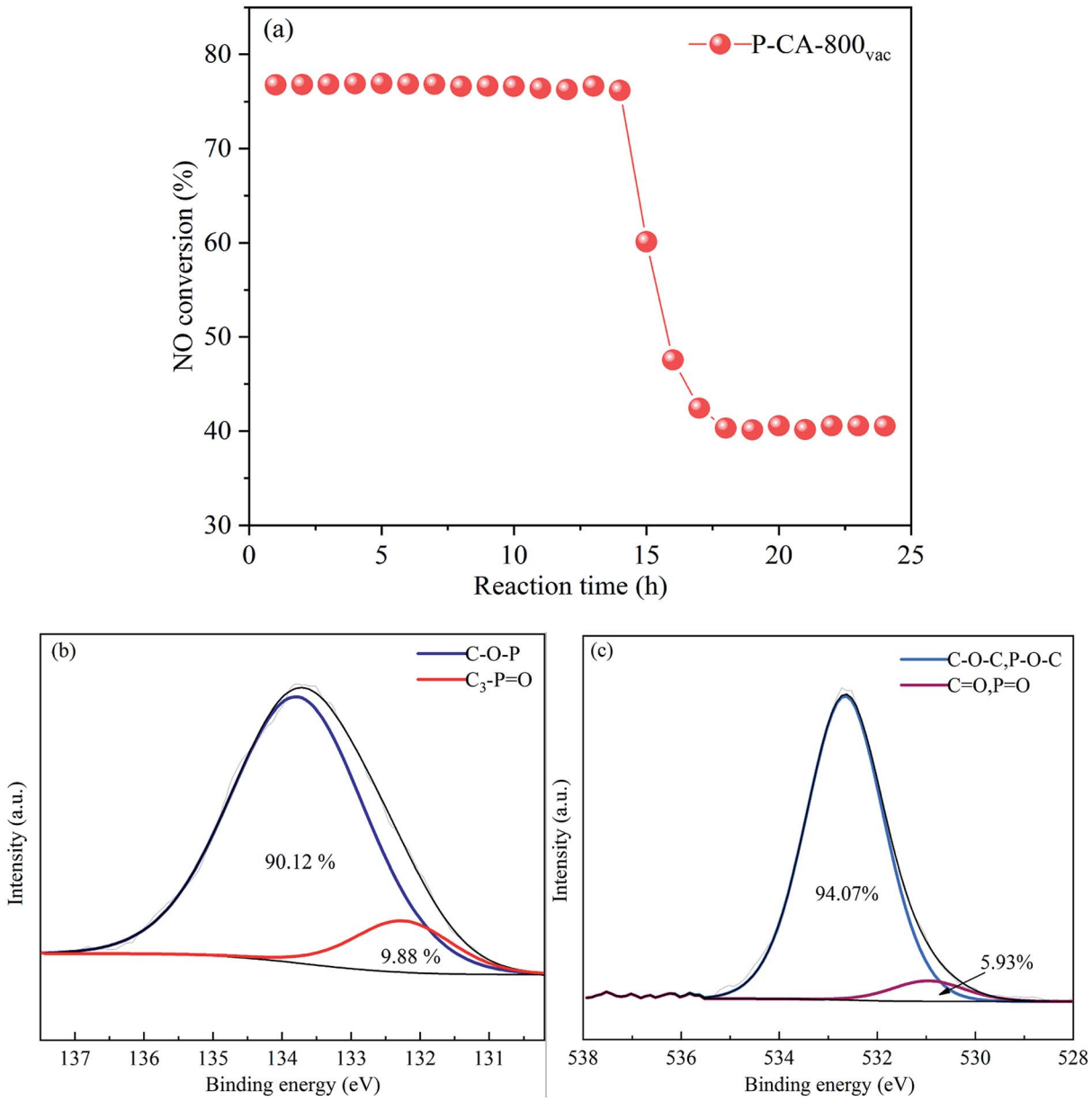

Fig. 6 (a) Stability test of NH_3-SCR for the P-CA-800_{vac} sample, (b) P2p and (c) O1s XPS spectra of the P-CA-800_{vac} after NH_3-SCR reaction for 24 h. Reaction conditions: [NO] = 500 ppm, [NH_3] = 500 ppm, [O_2] = 5%, N_2 balance, GHSV = 500 h^{-1}, 200 °C.

the results of DFT calculations based on the N-doped graphene.[15]

The introduction of NH_3 can further improve the NO conversion and decrease the spillover of NO_2 and N_2O, as shown in Fig. 7c. Based on the experimental results, a mechanism for NH_3-SCR of NO over P-CAs is proposed, as depicted in the eqn (7)–(10). Firstly, the O_2 molecular is adsorbed on the carbon regions activated by P-doping and dissociated to O* that can readily interact with NO to generate NO_2, meanwhile NH_3 can be coordinated on the Brønsted acid sites to form NH_4^+, then NO_2 can react with NH_4^+ to generate an ammonium nitrite intermediate,[23,24] which can decompose directly into N_2 and H_2O. Therefore, the simultaneous presence of acidic groups for NH_3 adsorption and the active sites for NO_2 generation due to activation of O_2 molecular should be responsible for the significant increase in SCR activity over the P–CAs as compared with the undoped one. In addition, the C_3–P=O groups transfer into C–O–P bonds after the stability test as revealed by the XPS results, which could be assigned to the oxidation of C_3–P=O by the dissociated O*, as described by the eqn (11)–(13). We propose a mechanism for structure evolution from C_3–P=O to C–O–P, as illustrated in Fig. 8. The dissociated O* atom could be easily adsorbed at the bridge site of C–P bonds of C_3–P=O configuration due to the accumulated electrons on the C–P bonds.[29] The highly reactive O* would attack the C–P bonds and insert into C–P bonds to form C–O–P bonds,[23,24] resulting in the deactivation of catalytic sites for SCR reaction. Besides, the oxidation of carbon may also occur as in other carbon materials

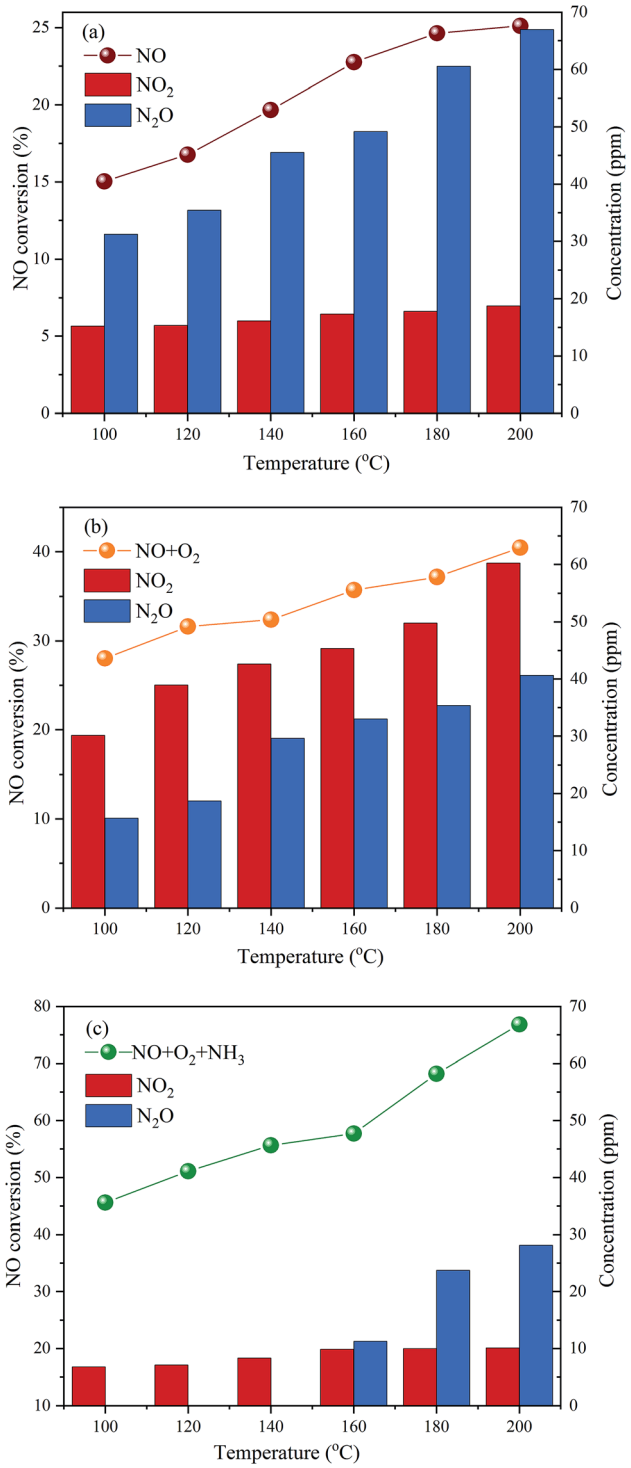

Fig. 7 NO conversions, NO_2 and N_2O concentration in the outlet gas over the P-CA-800_{vac} sample for the different inlet gases of NO, NO + O_2 and NO + NH_3 + O_2. Reaction conditions: [NO] = 500 ppm, [NH_3] = 500 ppm (when used), [O_2] = 5% (when used), N_2 balance, GHSV = 500 h^{-1}.

that can be described by the eqn (14).[10,17] Certainly, much more work is undergoing to elucidate the exact mechanism *via* a theoretical DFT calculation.

$$NO + NO \rightarrow (NO)_2(ad) \quad (4)$$

$$(NO)_2(ad) \rightarrow N_2O + O^*(ad) \quad (5)$$

$$N_2O \rightarrow N_2 + O^*(ad) \quad (6)$$

$$O^*(ad) + NO \rightarrow NO_2 \quad (7)$$

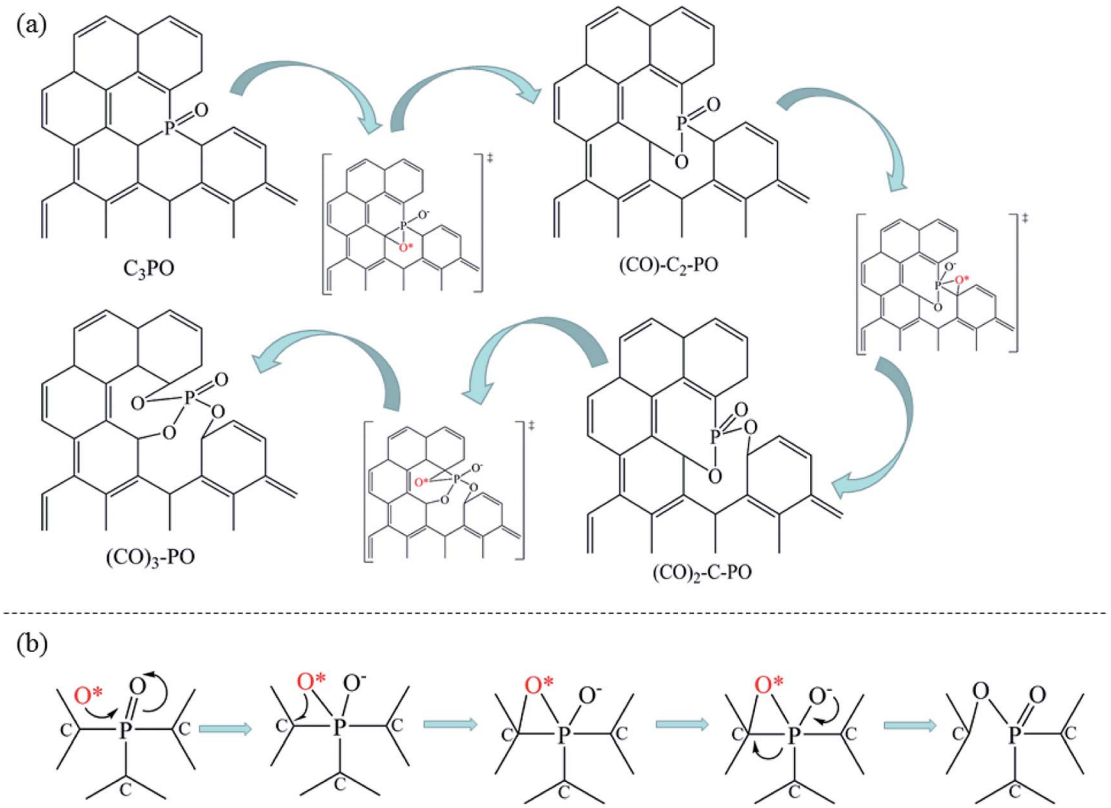

Fig. 8 Proposed mechanism for structure evolution from C_3–P=O to C–O–P.

$$O_2 \rightarrow O^*(ad) + O^*(ad) \quad (8)$$

$$NH_3 + H^+(\text{Brønsted acid sites}) \rightarrow NH_4^+(ad) \quad (9)$$

$$NH_4^+(ad) + NO_2 \rightarrow NH_4NO_2 \rightarrow N_2 + 2H_2O \quad (10)$$

$$-C_3P{=}O + O^*(ad) \rightarrow -CO{-}C_2{-}P{=}O \quad (11)$$

$$-CO{-}C_2{-}P{=}O + O^*(ad) \rightarrow -(CO)_2{-}C{-}P{=}O \quad (12)$$

$$-(CO)_2{-}C{-}P{=}O + O^*(ad) \rightarrow -(CO)_3{-}P{=}O \quad (13)$$

$$-C{-}C- + O^*(ad) \rightarrow CO(CO_2) \quad (14)$$

It should be noted that although the P-CA-800 has a low apparent activation energy and a high activity at low temperatures, its GHSV is only 500 h^{-1}, significantly lower than other inorganic oxide based catalysts. This could be caused by a small number of active species. Therefore, a further work is necessary to increase the number of active sites for this catalyst system.

4. Conclusion

This work studied the influence of P doping on the NH_3-SCR activity over carbon aerogels as a metal-free catalyst at low temperatures. The results show that the incorporated P species on the carbon sheets can effectively enhance the catalytic activity of carbon aerogels for NO reduction. The NH_3-TPD results show that Brønsted acid sites are introduced to the carbon surface due to mainly the presence of a large portion of C–OH and P–OH species, and a small portion of COOH group. Moreover, the C_3–P=O structure may act as the most active sites for easy adsorption and dissociation of O_2 to facilitate NO_2 generation. Therefore, the improvement of SCR activity over the P-CAs is assigned to simultaneous presence of acidic groups for NH_3 adsorption and the active sites for NO_2 generation due to activation of O_2 molecular. Based on the experimental results, a mechanism for NH_3-SCR of NO over the P-CAs is proposed. Firstly, the O_2 molecular is adsorbed on the carbon regions activated by P-doping and dissociated to O* that can readily interact with NO to generate NO_2, meanwhile NH_3 can be coordinated on the Brønsted acid sites to form NH_4^+, then NO_2 can react with NH_4^+ to generate an ammonium nitrite intermediate, which decomposes directly into N_2 and H_2O. The C_3–P=O configuration is unstable and oxidized to C–O–P groups probably by O_2 during reaction, leading to an apparent decrease of catalytic activity for P-CAs for a reaction time beyond 14 h. These results enrich the understanding on contributions of heteroatoms to the catalytic activity of carbon for the low-temperature NH_3-SCR reaction. More experimental and theoretical work will be done to demonstrate and improve the proposed mechanisms. Moreover, some efforts can be made to develop the oxidation resistance of the C–P bonds to enhance the durability of P-CA catalysts and to increase the number of active sites.

Conflicts of interest

There are no conflicts to declare.

Acknowledgements

This work was financially supported by the National Natural Science Foundation of China (No. U1710252).

References

1 Q. Zhao, J. Xiang, L. Sun, S. Su and S. Hu, *Energy Fuels*, 2009, **23**, 539–1544.
2 W. Shan and H. Song, *Catal. Sci. Technol.*, 2015, **5**, 4280–4288.
3 R. Jin, Y. Liu, Z. Wu, H. Wang and T. Gu, *Chemosphere*, 2010, **78**, 1160–1166.
4 Z. Liu, Y. Li, T. Zhu, H. Su and J. Zhu, *Ind. Eng. Chem. Res.*, 2014, **53**, 12964–12970.
5 Y. Yang, M. Wang, Z. Tao, Q. Liu, Z. Fei, X. Chen, Z. Zhang, J. Tang, M. Cui and X. Qiao, *Catal. Sci. Technol.*, 2018, **8**, 6396–6406.
6 S. Ahmed, R. Baldwin, F. Derbyshire, B. Mcenaney and J. Stencel, *Fuel*, 1993, **72**, 287–292.
7 B. Ku, J. Lee, D. Park and H. Rhee, *Ind. Eng. Chem. Res.*, 1994, **33**, 2868–2874.
8 J. Muniz, G. Marban and A. Fuertes, *Appl. Catal., B*, 1999, **23**, 25–35.
9 H. Teng, Y. Tu, Y. Lai and C. Lin, *Carbon*, 2001, **39**, 575–582.
10 J. Zhang, Q. Gao, X. Li, J. Zhou, X. Ruan, Q. Liu, G. Qian and Z. Xu, *Phys. Chem. Chem. Phys.*, 2017, **19**, 22462–22471.
11 J. Muñiz, G. Marbán and A. Fuertes, *Appl. Catal., B*, 2000, **27**, 27–36.
12 M. Huang and H. Teng, *Carbon*, 2003, **41**, 951–957.
13 G. Szymanski, T. Grzybek and H. Papp, *Catal. Today*, 2004, **90**, 51–59.
14 T. Grzybek, J. Klinik, B. Samojeden, V. Suprun and H. Papp, *Catal. Today*, 2008, **137**, 228–234.
15 X. Zhang, Z. Lu, Y. Tang, D. Ma and Z. Yang, *Catal. Lett.*, 2014, **144**, 1016–1022.
16 X. Zhang, Z. Lu, Y. Tang, Z. Fu, D. Ma and Z. Yang, *Phys. Chem. Chem. Phys.*, 2014, **16**, 20561–20569.
17 Y. Wang, Y. Shen and S. Zhu, *Catal. Commun.*, 2017, **9**, 29–32.
18 Y. Wang, Y. Shen, Y. Zhou, Z. Xue, Z. Xi and S. Zhu, *ACS Appl. Mater. Interfaces*, 2018, **10**, 36202–36210.
19 S. Ji and J. Zhao, *New J. Chem.*, 2018, **42**, 16346–16353.
20 D. Yang, D. Bhattacharjya, S. Inamdar, J. Park and J. Yu, *J. Am. Chem. Soc.*, 2012, **134**, 16127–16130.
21 W. He, Y. Wang, C. Jiang and L. Lu, *Chem. Soc. Rev.*, 2016, **45**, 2396–2409.
22 M. Patel, F. Luo, M. Khoshi, E. Rabie, Q. Zhang and C. Flach, *ACS Nano*, 2016, **10**, 2305–2315.
23 Z. Bi, L. Huo, Q. Kong, F. Li, J. Chen, A. Ahmad, X. Wei, L. Xie and C. Chen, *ACS Appl. Mater. Interfaces*, 2019, **11**, 11421–11430.
24 R. Berenguer, R. Ruiz-Rosas, A. Gallardo, D. Cazorla-Amorós, E. Morallón, H. Nishihara, T. Kyotani, J. Rodríguez-Mirasol and T. Cordero, *Carbon*, 2015, **95**, 681–689.
25 R. Li, Z. Wei, X. Gou and W. Xu, *RSC Adv.*, 2013, **3**, 9978–9984.
26 Y. Jiao, Y. Zheng, M. Jaroniec and S. Qiao, *J. Am. Chem. Soc.*, 2014, **136**, 4394–4403.
27 Y. Liu, K. Li, Y. Liu, L. Pu, Z. Chen and S. Deng, *J. Mater. Chem. A*, 2015, **3**, 21149–21158.
28 X. Zhang, Z. Lu, Z. Fu, Y. Tang, D. Ma and Z. Yang, *J. Power Sources*, 2015, **276**, 222–229.
29 N. Yang, X. Zheng, L. Li, J. Li and Z. Wei, *J. Phys. Chem. C*, 2017, **121**, 19321–19328.
30 R. Gao, L. Pan, J. Lu, J. Xu, X. Zhang, L. Wang and J. Zou, *ChemCatChem*, 2017, **9**, 4287–4294.
31 R. Gao, L. Pan, Z. Li, X. Zhang, L. Wang and J. Zou, *Chin. J. Catal.*, 2018, **39**, 664–672.
32 R. Huang, J. Wang, B. Zhang, K. Wu, Y. Zhang and D. Su, *Catal. Sci. Technol.*, 2018, **8**, 1522–1527.
33 J. Liu, X. Li, Q. Zhao, J. Ke, H. Xiao, X. Lv, S. Liu, M. Tadé and S. Wang, *Appl. Catal., B*, 2017, **200**, 297–308.
34 Y. Peng, K. Li and J. Li, *Appl. Catal., B*, 2013, **140**, 483–492.
35 Y. Wang, S. Zuo, J. Yang and J. Yoon, *Langmuir*, 2017, **33**, 3112–3122.
36 X. Wu and L. Radovic, *Carbon*, 2006, **44**, 141–151.
37 J. Rosas, J. Bedia, J. Rodríguez-Mirasol and T. Cordero, *Fuel*, 2009, **88**, 19–26.
38 A. Puziy, O. Poddubnaya, R. Socha, J. Gurgul and M. Wisniewski, *Carbon*, 2008, **46**, 2113–2123.
39 M. Patel, F. Luo, M. Khoshi, E. Rabie, Q. Zhang, C. Flach, R. Mendelsohn, E. Garfunkel, M. Szostak and H. He, *ACS Nano*, 2016, **10**, 2305–2315.
40 W. Ma, L. Xie, L. Dai, G. Sun, J. Chen, F. Su, Y. Cao, H. Lei, Q. Kong and C. Chen, *Electrochim. Acta*, 2018, **266**, 420–430.
41 M. Valero-Romero, F. García-Mateos, J. Rodríguez-Mirasol and T. Cordero, *Fuel Process. Technol.*, 2017, **157**, 116–126.
42 G. Dong, Y. Zhang, Y. Zhao and Y. Bai, *J. Fuel Chem. Technol.*, 2014, **42**, 1455–1463.
43 L. Gan, F. Guo, J. Yu and G. Xu, *Catalysts*, 2016, **6**, 25.
44 I. Mejri, F. Ayari, M. Mhamdi, G. Ksibi and A. Ghorbel, *Microporous Mesoporous Mater.*, 2016, **220**, 239–246.
45 A. Chughtai, M. Atteya, J. Kim, B. Konowalchuk and D. Smith, *Carbon*, 1998, **36**, 1573–1589.
46 G. Marbán, T. Valdés-Solís and A. Fuertes, *J. Catal.*, 2004, **226**, 138–155.
47 C. Liu, J. Shi, C. Gao and C. Niu, *Appl. Catal., A*, 2016, **522**, 54–69.
48 L. Kang, L. Han, J. He, H. Li, T. Yan, G. Chen, J. Zhang, L. Shi and D. Zhang, *Environ. Sci. Technol.*, 2019, **53**, 938–945.
49 Z. Hao, Z. Shen, Y. Li, H. Wang, L. Zheng, R. Wang, G. Liu and S. Zhan, *Angew. Chem.*, 2019, **58**, 6351–6356.
50 K. Ramesh, C. Jie, Y. Han and A. Borgna, *Ind. Eng. Chem. Res.*, 2010, **49**, 4080–4090.
51 J. Bedia, J. Rosas, D. Vera, J. Rodríguez-Mirasol and T. Cordero, *Catal. Today*, 2010, **158**, 89–96.
52 J. Bedia, R. Ruiz-Rosas, J. Rodríguez-Mirasol and T. Cordero, *J. Catal.*, 2010, **271**, 33–42.

53 B. Maia, J. Tjong and M. Sain, *Materials Today Sustainability*, 2019, **5**, 100011.
54 M. Guerrero-Pérez, M. Valero-Romero, S. Hernández, J. Nieto, J. Rodríguez-Mirasol and T. Cordero, *Catal. Today*, 2012, **195**, 155–161.
55 A. Puziy, O. Poddubnaya, A. Martínez-Alonso, A. Castro-Muñiz, F. Suárez-García and J. Tascón, *Carbon*, 2007, **45**, 1941–1950.
56 H. Wang, H. Wang, Y. Chen, Y. Liu, J. Zhao, Q. Cai and X. Wang, *Appl. Surf. Sci.*, 2013, **273**, 302–309.
57 I. Mochida, N. Shirahama, S. Kawano, Y. Korai, A. Yasutake, M. Tanoura, S. Fujii and M. Yoshikawa, *Fuel*, 2000, **79**, 1713–1723.
58 Z. Guo, Y. Xie, I. Hong and J. Kim, *Energy Convers. Manage.*, 2001, **42**, 2005–2018.
59 J. Sousa, M. Pereira and J. Figueiredo, *Catal. Today*, 2011, **176**, 383–387.
60 S. Adapa, V. Gaur and N. Verma, *Chem. Eng. J.*, 2006, **116**, 25–37.
61 W. Zhang, S. Rabiei, A. Bagreev, M. Zhuang and F. Rasouli, *Appl. Catal., B*, 2008, **83**, 63–71.
62 Z. Zhang, J. Atkinson, B. Jiang, M. Rood and Z. Yan, *Appl. Catal., B*, 2014, **148**, 573–581.